Reductive Self-assembling of Pd and Rh Nanoparticles on Silicon Nanowire Templates

Xu-Hui Sun,[†] Ning-Bew Wong,*[,‡,§] Chi-Pui Li,[‡,||] Shuit-Tong Lee,[‡,||] Pil-Sook G. Kim,[†] and Tsun-Kong Sham*[,†]

Department of Chemistry, University of Western Ontario, London, Canada N6A 5B7, Center of Super-Diamond & Advanced Film (COSDAF), Department of Biology and Chemistry, and Department of Physics and Materials Science, City University of Hong Kong, Hong Kong

Received November 3, 2003. Revised Manuscript Received January 15, 2004

Palladium and rhodium nanoparticles have been reductively fabricated on the hydrogen-passivated surfaces of silicon nanowires (SiNWs), which exhibited moderate reactivity toward the reduction of Pd(II) and Rh(III) to metal in aqueous solution. We observed, with high-resolution transmission electron microscopy (HRTEM), the formation of nanoparticles of different shapes, such as round, elliptic, polyhedral, and so forth, on the SiNW surfaces, depending on the size of these metal nanoparticles. Two interesting phenomena, "nanoparticle departure" and "nanoparticle submersion" attributable to nanoparticle interface oxide interaction as well as some interesting structures self-assembled by the nanoparticles and the SiNWs, were observed under HRTEM. The electronic properties and local structure of these metal nanoparticles and the SiNWs templates have been investigated by X-ray absorption fine structures. The Pd and Rh nanoparticles with a small diameter (<5 nm) showed a noticeable size effect.

I. Introduction

Nanotechnology is the culmination of many facets of developments in the nanorealm, including nanofabrication, nanomachineries, quantum devices, molecular machines, molecular computers, and so forth. The first steps toward building such nanodevices are the synthesis and characterization of nanomaterials and the study of their chemical and physical properties. In this regard, there has been a great deal of interest recently in the fabrication and characterization of nanostructures such as nanoparticles, nanotubes, and nanowires. The electronic, magnetic, mechanical, and chemical properties of the nanoscale materials can differ significantly from their corresponding bulk counterparts due to the quantum size and the surface effects. In the past several years, many fabrication strategies such as colloidal chemistry and electrodeposition methods have been developed to fabricate metal nanoparticles such as Au, Pd, Ag, and Cu.[1−6] Recently, a hard nanotemplate approach has been developed to fabricate metal nanoparticles, utilizing porous silicon as a moderate reducing agent and a nanostructure template for the reductive formation of Cu, Rh, Pd, Ag, Pt, and Au nanoparticles in aqueous solutions of their metal ions.[7−12]

Silicon is of great technological importance in microelectronics. Considerable advances have been made on the fabrication, characterization, and properties of silicon nanowires (SiNWs).[13−31] Many successful syn-

* To whom correspondence should be addressed. E-mail: sham@uwo.ca (T.-K. Sham); bhnbwong@cityu.edu.hk (N.-B. Wong).
[†] University of Western Ontario.
[‡] Center of Super-Diamond & Advanced Film, City University of Hong Kong.
[§] Department of Biology and Chemistry, City University of Hong Kong.
[||] Department of Physics and Materials Science, City University of Hong Kong.

(1) Leff, D. V.; Ohara, P. C.; Heath, J. R.; Gelbart, W. M. *J. Phys. Chem.* **1995**, *99*, 7036.
(2) Templeton, A. C.; Chen, S.; Gross, S. M.; Murray, R. W. *Langmuir* **1999**, *15*, 66.
(3) Chen, S.; Huang, K.; Stearn, J. A. *Chem. Mater.* **2000**, *12*, 540.
(4) Kang, S. Y.; Kim, K. *Langmuir* **1998**, *14*, 226.
(5) Chen, S.; Sommers, J. M. *J. Phys. Chem. B* **2001**, *105*, 8816.
(6) Zhang, P.; Sham, T. K. *Phys. Rev. Lett.* **2003**, *90*, 245502−245504.
(7) Coulthard, I.; Jiang, D. T.; Lorimer, J. W.; Sham, T. K.; Feng, X. H. *Langmuir* **1993**, *9*, 3441.
(8) Sham, T. K.; Coulthard, I.; Lorimer, J. W.; Hiraya, A.; Watanabe, M. *Chem. Mater.* **1994**, *6*, 2085.
(9) Coulthard, I.; Sham, T. K. *Solid State Commun.* **1998**, *105*, 751.
(10) Coulthard, I.; Zhu, Y. J.; Degan, S.; Sham, T. K. *Can. J. Chem.* **1999**, *76*, 1707.
(11) Zhu, Y. J.; Coulthard, I.; Sham, T. K. *J. Synchrotron Radiat.* **1999**, *6*, 529.
(12) Coulthard, I.; Sammynaiken, R.; Naftel, S. J.; Zhang, P.; Sham, T. K. *Phys. Status Solidi A* **2000**, *182*, 157.
(13) Zhang, Y. F.; Tang, Y. H.; Wang, N.; Yu, D. P.; Lee, C. S.; Bello, I.; Lee, S. T. *Appl. Phys. Lett.* **1998**, *72*, 1835−1837.
(14) Morales, A. M.; Lieber, C. M. *Science* **1998**, *279*, 208−211.
(15) Yu, D. P.; Bai, Z. G.; Ding, Y.; Hang, Q. L.; Zhang, H. Z.; Wang, J. J.; Zou, Y. H.; Qian, W.; Xiong, G. C.; Zhou, H. T.; Feng, S. Q. *Appl. Phys. Lett.* **1998**, *283*, 3458−3460.
(16) Wang, N.; Tang, Y. H.; Zhang, Y. F.; Yu, D. P.; Lee, C. S.; Bello, I.; Lee, S. T. *Chem. Phys. Lett.* **1998**, *283*, 368−372.
(17) Shi, W. S.; Peng, H. Y.; Zheng, Y. F.; Wang, N.; Shang, N. G.; Pan, Z. W.; Lee, C. S.; Lee, S. T. *Adv. Mater.* **2000**, *12*, 1343−1345
(18) Tang, Y. H.; Zhang, Y. F.; Wang, N.; Lee, C. S.; Han, X. D.; Bello, I.; Lee, S. T. *J. Appl. Phys.* **1999**, *85*, 7981−7983.
(19) Au, C. K. F.; Wong, K. W.; Tang, Y. H.; Zhang, Y. F.; Bello, I.; Lee, S. T. *Appl. Phys. Lett.* **1999**, *75*, 1700−1702.
(20) Volz, S. G.; Chen, G. *Appl. Phys. Lett.* **1999**, *75*, 2056−2058.
(21) Lee, S. T.; Wang, N.; Zhang, Y. F.; Tang, Y. H. *MRS Bull.* **1999**, 36−42.
(22) Cui, Y.; Duan, X.; Hu, J.; Lieber, C. M. *J. Phys. Chem. B* **2000**, *104*, 5213−5216.
(23) Cui, Y.; Lieber, C. M. *Science* **2001**, *291*, 851−853
(24) Zhang, Y. F.; Liao, L. S.; Chan, W. H.; Lee, S. T.; Sammynaiken, R.; Sham, T. K. *Phys. Rev. B* **2000**, *61*, 8296−8305.

10.1021/cm035112e CCC: $27.50
Published on Web 02/14/2004

thetic strategies have now been developed to obtain bulk quantities of SiNWs, using both gas-phase and condensed-phase techniques.[13−17] A number of properties such as the morphology, structure, photoluminescence, electron field emission, thermal and electronic conductivity, and surface chemistry of SiNWs have been studied.[18−31] The SiNWs are pseudo-one-dimensional wires of silicon with diameters of the order of nanometers, which can be synthesized by either thermal evaporation of SiO[17,21] or laser ablation of silicon targets in the presence of metal catalysts.[14] The SiNWs used in this work were prepared by the thermal evaporation of SiO without metal catalysts. The as-synthesized SiNWs are relatively inert due to the silicon oxide sheathing. The outer oxide layer can be removed by a controlled HF treatment. The surfaces of the HF-etched, oxide-free SiNWs have been found to be passivated by hydrogen (i.e., SiH_x species, where $x = 1-3$)[30,31] and exhibit moderately high reactivity in solution as a reducing agent.[25,27−29] Recently, the study of the reaction of SiNWs with a number of metal ions such as silver and copper in aqueous solution produces metal nanoparticles[25,27] and the reductive growth of nanosized Au−Ag clusters on HF-etched SiNWs in organic solvents have also been reported.[28] The HF-etched SiNWs can readily reduce silver, copper ions, and ligated Au−Ag clusters to metal nanoparticles on the surfaces of SiNWs at room temperature with concomitant reoxidation of the SiNW surface. By variation of the concentration of the metal ions in the solution, the nanostructures of these metals with different shapes and sizes can be obtained. These nanosystems will generally exhibit electronic properties different from those of the bulk materials. By reductively depositing the metal nanoparticles on the surfaces of SiNWs in the solution at room temperature, we assembled these metal nanoparticles, which may be considered as zero-dimensional "nanodots," on one-dimensional "nanowires".[28] It is believed that the fabrication of such metallic nanodots on silicon nanowires, for example, will eventually lead to new and novel composite materials of importance in nanotechnology.

In this paper, the palladium and rhodium nanoparticles were reductively fabricated on the surfaces of HF refreshed SiNWs. The HF treatment effectively removed the oxide layer. The formation and morphologies of the Pd and Rh nanoparticles were revealed by scanning electron microscopy (SEM) and high-resolution transmission electron microscopy (HRTEM). The interesting phenomena of the "nanoparticle departure" and "nanoparticle submersion" processes induced by electron bombardment under HRTEM and some interesting structures self-assembled by the nanoparticles and SiNWs are reported. The electronic properties and local structures of metal nanoparticles and the SiNWs have been investigated by X-ray absorption fine structure (XAFS) at the Pd $L_{3,2}$-edge, Rh $L_{3,2}$- and K-edge, and Si K-edge.

II. Experimental Section

SiNWs were synthesized by thermal evaporation techniques as described previously.[17,21] The as-synthesized SiNWs are long (micrometers), free-standing wires with a diameter of several nanometers to tens of nanometers, depending on the preparation conditions, and are usually encapsulated by a silicon oxide layer. The as-prepared SiNWs are relatively inert due to the relatively thick encapsulating silicon oxide layer. The oxide layer was removed by immersing the as-prepared SiNWs in a 5% HF solution for 5 min. The HF-etched SiNWs were then rinsed with deionized water. After HF etching, Pd and Rh depositions were carried out by exposing the SiNWs to droplets (∼0.1 mL) of either K_2PdCl_4 or Na_3RhCl_6 aqueous solutions, of different concentrations. The reaction products were examined with a scanning electron microscope (SEM), which was equipped with energy-dispersive X-ray spectroscopy (EDS), and a high-resolution transmission electron microscope (HRTEM) (Philips CM200 FEG) operated at 200 kV. X-ray absorption measurements were made immediately after each step of the procedure. Room-temperature X-ray absorption experiments were carried out at the Double Crystal Monochromator (DCM) beamline of the Canadian Synchrotron Radiation Facility (CSRF) located at the Synchrotron Radiation Center (SRC), University of Wisconsin-Madison. SRC is an 800 MeV/1 GeV, second-generation storage ring operating at ∼250-mA injection current. The DCM at SRC with InSb(111) crystals and a post-mirror at 3.5-keV cutoff provide an excellent match of optics and source for Si K-edge measurements[32] and are ideally suited for the study of Si K-edge and Pd and Rh $L_{3,2}$-edge of Pd/SiNW and Rh/SiNW. The monochromator was calibrated with Pd and Rh foils at their L_3-edge. The nanostructure results from HRTEM were also checked with the Rh K-edge Extended X-ray Absorption Fine Structures (EXAFS) conducted at the PNC-CAT (Pacific Northwest Consortium-Collaborative Access Team) BM beamline at the 7 GeV Advanced Photon Source (APS) located at Argonne National Laboratory.

III. Results and Discussion

III. a. Surface Chemistry. It is well-recognized that the as-prepared SiNWs have a relatively thick oxide layer. Its presence has been associated with the preferred linear growth of the SiNWs.[21] On the basis of the HRTEM results[28] and the X-ray absorption fine structure (XAFS) results,[27] the morphology and structure of crystalline silicon in SiNWs are found to remain intact after the removal of the surface oxide layer via a controlled HF treatment. It has also been observed by STM[31] and FTIR[30] that the Si surface dangling bonds were passivated by hydrogen, forming $-SiH_x$ ($x = 1-3$) on the SiNW surfaces. The presence of these hydrides on the Si(100) surface is well-documented. [33] The hydrogen-passivated surface showed a relatively good stability in air and in organic solvents under an ambient environment.[29,30,31] However, the hydrogen-passivated

(25) Sun, X. H.; Tang, Y. H.; Zhang, P.; Naftel, S.; Sammynaiken, R.; Sham, T. K.; Zhang, Y. F.; Peng, H. Y.; Wong, N. B.; Lee, S. T. *J. Appl. Phys.* **2001**, *90*, 6379−6383.
(26) Sun, X. H.; Peng, H. Y.; Tang, Y. H.; Shi, W. S.; Wong, N. B.; Lee, C. S.; Lee, S. T.; Sham, T. K. *J. Appl. Phys.* **2001**, *89*, 6396−6398.
(27) Sun, X. H.; Sammynaiken, R.; Nafte, S. J.; Tang, Y. H.; Zhang, P.; Kim, P. S.; Sham, T. K.; Fan, X. H.; Zhang, Y. F.; Wong, N. B.; Lee, C. S.; Lee, S. T.; Hu, Y. F.; Tan, K. H. *Chem. Mater.* **2002**, *14*, 2519−2526.
(28) Sun, X. H.; Li, C. P.; Wong, N. B.; Lee, C. S.; Lee, S. T.; Teo, B. K. *Inorg. Chem.* **2002**, *41*, 4331−4336.
(29) Sun, X. H.; Li, C. P.; Wong, N. B.; Lee, C. S.; Lee, S. T.; Teo, B. K. *J. Am. Chem. Soc.* **2002**, *124*, 14856−14857.
(30) Sun, X. H.; Wang, S. D.; Wong, N. B.; Ma, D. D. D.; Lee, S. T.; Teo, B. K. *Inorg. Chem.* **2003**, *42*, 2398−2404.
(31) Ma, D. D. D.; Lee, C. S.; Au, F. C. K.; Tong, S. Y.; Lee, S. T. *Science* **2003**, *299*, 1874−1877.
(32) Yang, B. X.; Middleton, H. F.; Olson, B. G.; Bancroft, G. M.; Chen, J. M.; Sham, T. K.; Tan, K. H.; Wallace, D. J. *Nucl. Instrum. Methods* **1992**, *316*, 422.
(33) Lu, Z. H.; Griffiths, K.; Norton, P. R.; Sham, T. K. *Phys. Rev. Lett.* **1992**, *68*, 1343−1346.

Scheme 1. Reaction Pathway of SiNWs and Pd(II) and Rh(III) Solutions

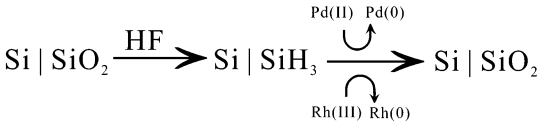

surface of SiNWs is a modest reducing agent in aqueous solution. In the presence of metal ions such as Ag(I), Cu(II),[25] Pd(II), and Rh(III), the SiNW surface serves both as a reducing agent and a nanotemplate substrate, which can readily reduce these metal ions to metal nanostructures at room temperature, becoming reoxidized in the process. The reaction pathway is shown in Scheme 1. Here the vertical lines represent schematically the interface between the crystalline silicon lattice at the core and the amorphous silicon dioxide layer on the surface of the SiNW. Etching the SiNWs with a dilute HF solution removes the oxide layer. The HF-etched SiNW surface is hydrogen-passivated and can reduce a Pd(II) and Rh(III) ions in solution to metal Pd(0) and Rh(0) and further grow to nanoparticles on the surfaces of SiNWs. In the process, the SiNW surface is reoxidized. The reactions between Si wafer and metal ions have been studied in the process of the metal contamination of the Si wafer surface in solutions. The Si wafer cannot reduce the metal ions in the simple metal ion aqueous solution systems as in our studies except in the presence of HF in the solution or in other complex buffer systems.[34,35] However, interaction of SiNWs with metal ions in solution is a complex surface electrochemistry process. Although a plausible reaction mechanism can be deduced from the reaction products, the reaction mechanism needs to be confirmed by further studies. The reduction of metal ions and the oxidation of surface Si involve electron transfer to the metal ions absorbed on the surface of SiNWs from the surface atom; meanwhile, the hydride is oxidized to form hydrogen gas simultaneously in the presence of the catalytic metal[36] (bubbles were observed when relatively large quantities of SiNWs were dipped in the Pd(II) and Rh(III) solutions). We propose the oxidation and reduction half reactions in Pd/Rh−SiNWs systems below:

$$\text{oxidation: } \mathrm{Si{-}H_x + H_2O \rightarrow SiO_2 + (\mathit{X}/2)H_2 + 4H^+ + 4e^-}$$

$$\mathrm{Si + H_2O \rightarrow SiO_2 + 4H^+ + 4e^-}$$

$$\text{reduction: } \mathrm{Pd^{2+} + 2e^- \rightarrow Pd}$$

$$\mathrm{Rh^{3+} + 3e^- \rightarrow Rh}$$

The above-described pathway is supported by a significant decrease in the pH of the residue solution, as was in the case of similar processes involving porous silicon.[7−9] By varying the concentration of the metal ions in solution, we can anchor nanostructures of metals with different shapes and sizes on the SiNW surfaces, which serve as the nanotemplates. There has been ample evidence from porous silicon studies showing that both the hydrides and the zero-valence Si participate in the process resulting in the re-oxidation of the surface silicon.[9−12]

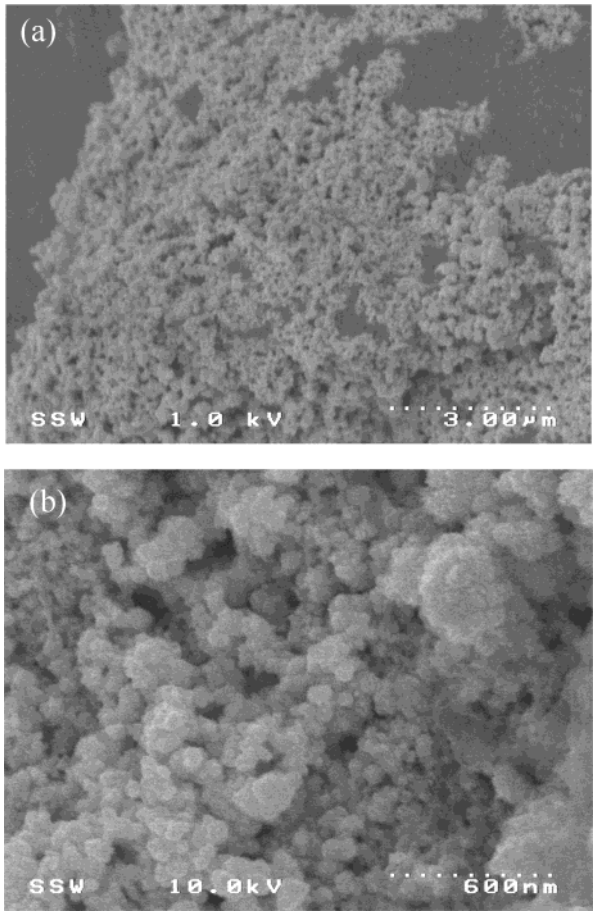

Figure 1. (a) SEM image of Pd nanoparticles aggregates on SiNWs from reductive deposition in a 1.0×10^{-3} M Pd(II) solution. (b) High magnification of SEM image of (a).

III. b. Morphologies and Self-assembling of Pd and Rh Nanoparticles on SiNW Surfaces. Figure 1a shows the SEM image of Pd nanoparticles aggregated on SiNWs from the reductive deposition of Pd(II) in a 1.0×10^{-3} M solution. High magnification, Figure 1b, reveals a distribution of aggregates varying from tens of nanometers to hundreds of nanometers. The presence of Pd is also confirmed with EDS. The TEM images of Pd nanoparticles on SiNWs from the 1.0×10^{-4}M Pd(II) solution are shown in Figure 2a. The size of most of the Pd nanoparticles is smaller than 5 nm. The HRTEM image shown in Figure 2b reveals the detailed crystalline structure of these Pd nanoparticles. They are either attached to the SiNWs, which have a 3.1 Å spacing of the Si{111} planes, or immersed in the amorphous SiO_2, whereas these particles have a 2.2-Å lattice spacing indicating that the particles are Pd with a face-centered cubic (fcc) structure. Similar results were obtained for Rh. We found that no Pd and Rh nanoparticles larger than 10 nm were attached to the SiNW surface. As the metal nanoparticles grew to a larger size (>10 nm in diameter), they tended to separate from the SiNW surfaces. This phenomenon was previously observed in the reaction of Au−Ag clusters on the SiNW surfaces.[28]

(34) Ohmi, T.; Imaoka, T.; Sugiyama, I.; Kezuka, T. *J. Electrochem. Soc.* **1992**, *139*, 3317.
(35) Nagahara, L. A.; Ohmori, T.; Hashimoto, K.; Fujishima, A. *J. Vac. Sci. Technol.* A **1993**, *11*, 763.
(36) Jeske, M.; Schultze, J. W.; Thönissen, M.; Münder, H. *Thin Solid Films* **1995**, *255*, 63.

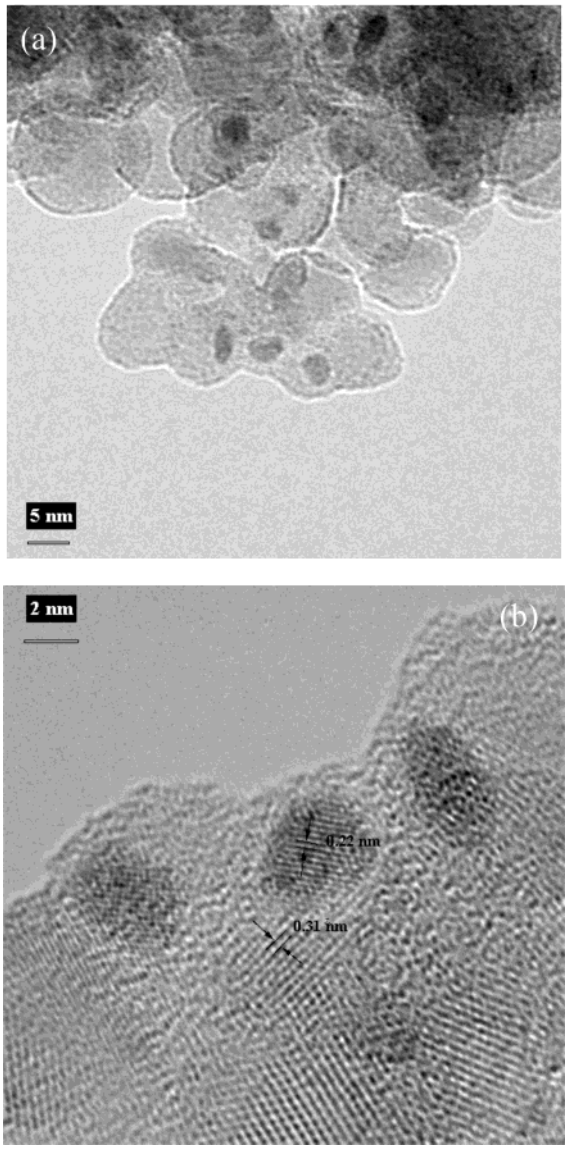

Figure 2. (a) TEM image of Pd nanoparticles on SiNWs formed in 1.0×10^{-4} M Pd(II) solution. (b) HRTEM image of Pd nanoparticles in (a).

The morphologies of Pd and Rh nanoparticles on the SiNW surfaces were observed. There are generally two types: those that are protected with an oxide layer and those that are not. Figure 3 depicts a typical round-shaped Rh nanoparticle with an 8-nm diameter attached onto a SiNW surface. It appears that, in general, the round-shaped nanoparticles have a larger diameter (4−10 nm) and are covered by a thin amorphous oxide layer. This thin oxide layer was probably formed after the formation of these metal nanoparticles, which were either oxidized in the air when the sample was stored in air or reacted with silicon oxide in the vicinity. The latter process is more reasonable because some smaller metal nanoparticles (<5 nm) without an oxide layer were also observed (see below). In the reduction and the growth process of the nanoparticles on the HF-etched SiNW surfaces, silicon oxides were formed on the SiNW surface as the surface silicon atoms acted as a reducing agent and got reoxidized in the process. Consequently, some of these nanoparticles were partially or completely surrounded by a silicon oxide layer, thereby appearing to be partially or completely capped by the oxide. In this

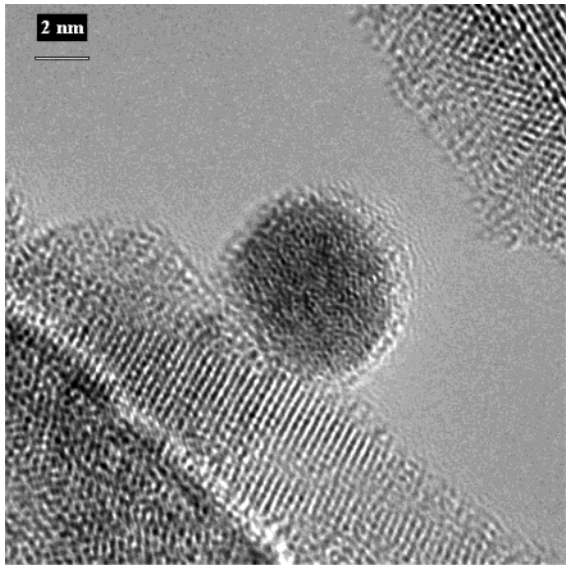

Figure 3. HRTEM image of a round Rh nanoparticle of 8 nm on a SiNW surface.

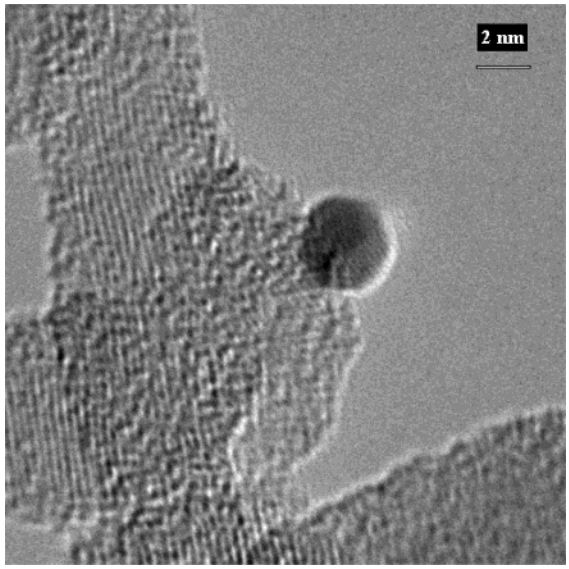

Figure 4. HRTEM image of one perfect individual polyhedra Rh particle of about 3.5 nm on a SiNW surface.

regard, the oxides served as the capping ligands, stabilizing the metal nanoparticles on the SiNW surfaces. This type of nanoparticles showed good stability under HRTEM observation. This observation is in good agreement with a similar observation made in the study of the deposition of Au−Ag alloy nanoparticles on SiNW surfaces.[28]

Many of the smaller nanoparticles (<5 nm) exhibit well-defined facets, suggesting a high-frequency polyhedral structure as illustrated by the HRTEM image of such an Rh particle shown in Figure 4. The HRTEM images for the Pd nanoparticles are shown in Figure 5a and Figure 6a. The Rh nanoparticle appears to be an individual polyhedron of about 3.5 nm in diameter. Both Rh and Pd nanoparticles noted here exhibited a clear fcc lattice structure without an amorphous oxide layer boundary under HRTEM observation. However, this type of nanoparticle (no capping) showed poor stability under intense TEM electron beam bombardment. It was found that some metal nanoparticles

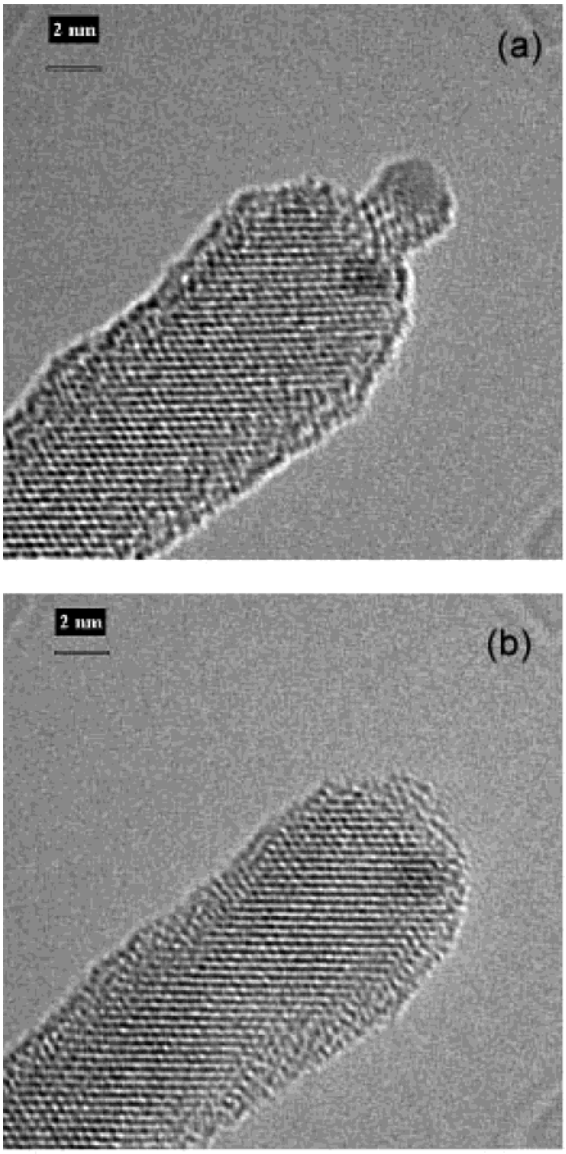

Figure 5. HRTEM image of the "departing nanoparticle" process (a) in the beginning of the HRTEM observation and (b) after a few seconds.

attached on the SiNW surface were departing from the SiNW surface or sinking into the amorphous oxide layer during TEM observation. We term the former phenomenon "nanoparticle departure" and the latter "nanoparticle submersion".

Two snapshots of the process of "nanoparticle departure" and four snapshots of the entire process of "nanoparticle submersion" are depicted in Figure 5 and Figure 6, respectively. In Figure 5a, the Pd nanoparticle of approximately 2 nm in diameter attached on the tip of a SiNW was seen to throb under the intense electron beam of the TEM. After a few seconds, the particle separated abruptly from the tip of the SiNW, (Figure 5b). In another case, the particle gradually sank beneath the surface of the oxide layer as shown in Figure 6, in which a Pd nanoparticle of 3 nm in diameter is seen adhered to the tip of a SiNW (Si oxide layer) in Figure 6a. Under the intense e-beam of TEM, the particle throbbed and then started to roll over the surface and moved rapidly to a neighboring SiNW (Figure 6b,c). Subsequently the particle began to submerge beneath the surface of the oxide layer. And, after about 1 min, the particle submersed in the oxide layer (Figure 6d). This process is accompanied by a gradual but clearly noticeable reduction in the size of the nanoparticle. A similar phenomenon was recently observed when Au−Ag alloy clusters were deposited on SiNW[28] and magnesium oxide.[37,38] We propose that, in all cases, the oxide−nanoparticle interface plays an important role in the nanoparticle "departure" and "submission" processes. In other words, under the irradiation of the intense electron beam, the small metal nanoparticles without any ligand protection were unstable. Nanoparticles on the surface of SiNWs without much oxide were blown away by the irradiation of the intense electron beam (as observed in Figure 5). However, if there is an oxide layer, the oxide will react with the nanoparticles, ripping off some of the surface atoms from the nanoparticle in the process, ultimately forming an oxide-capped nanoparticle. This process is likely to be facilitated by the diffusion of Rh or Pd into the SiNW and the tendency to form metal silicide. This explains the reduction in nanoparticle size from ∼3 nm (Figure 6a) to ∼1.5 nm (Figure 6d). Phenomenologically, the metal nanoparticle "sank" into the oxide layer; some completely submersed, while others only partially. Obviously, the anchoring and the engulfing of the metal clusters on the surfaces of the SiNWs upon heating locally by the TEM electrons depend critically on the local morphology, and the interaction between the metal nanoparticle surfaces and the substrate, and hence are intimately related to the processes such as adhesion and wetting.[39]

Some other shapes of the nanoparticles were also observed. An elliptical Pd nanoparticle with a short axis of 4 nm and a long axis of 6 nm is shown in Figure 7, where the nanoparticle shows a 0.22-nm *d* spacing, characteristic of an fcc lattice structure. Some smaller nanoparticles form aggregates. An aggregate of several Rh nanoparticles of about 2 nm in diameter was found attached onto the surface oxide of SiNW, as depicted in Figure 8. Still other interesting structures self-assembled by the nanoparticles and SiNWs were worth noting. Figure 9 shows an Rh nanoparticle "hanging" on the body of a SiNW. Another round Rh nanoparticle of 3-nm nanoparticle was sandwiched between two SiNWs, as shown in Figure 10. These self-assembled structures of metal nanodots and semiconductor nanowires have interesting implications to future fabrication of nanodevices. However, how to specifically place metal nanodots of a predetermined size on silicon nanowires and further self-assemble a specific nanostructure need further work.

III. c. XAFS of the Pd and Rh Nanoparticles and the SiNW Substrate. Figure 11a shows the Pd $L_{3,2}$ near-edge spectra of Pd/SiNW compared with that of a Pd metal, where the edge jumps of the 1.0×10^{-3} and 1.0×10^{-4} M samples have been multiplied by 10 and 20, respectively. It should be noted that XAFS measurements sample the average of all nanoparticles in the specimen examined by the photon beam (mm in size). A more detailed comparison of the Pd L_3-edge of these

(37) Marks, L. D.; Hong, M. C.; Zhang, H.; Teo, B. K. *Mater. Res. Soc. Symp. Proc.* **1989**, *111*, 213−218.
(38) Ajayan, P. M.; Marks, L. D. *Nature* **1989**, *338*, 139−141.
(39) Iijima, S.; Ichihashi, T. *Phys. Rev. Lett.* **1986**, *56*, 616−619.

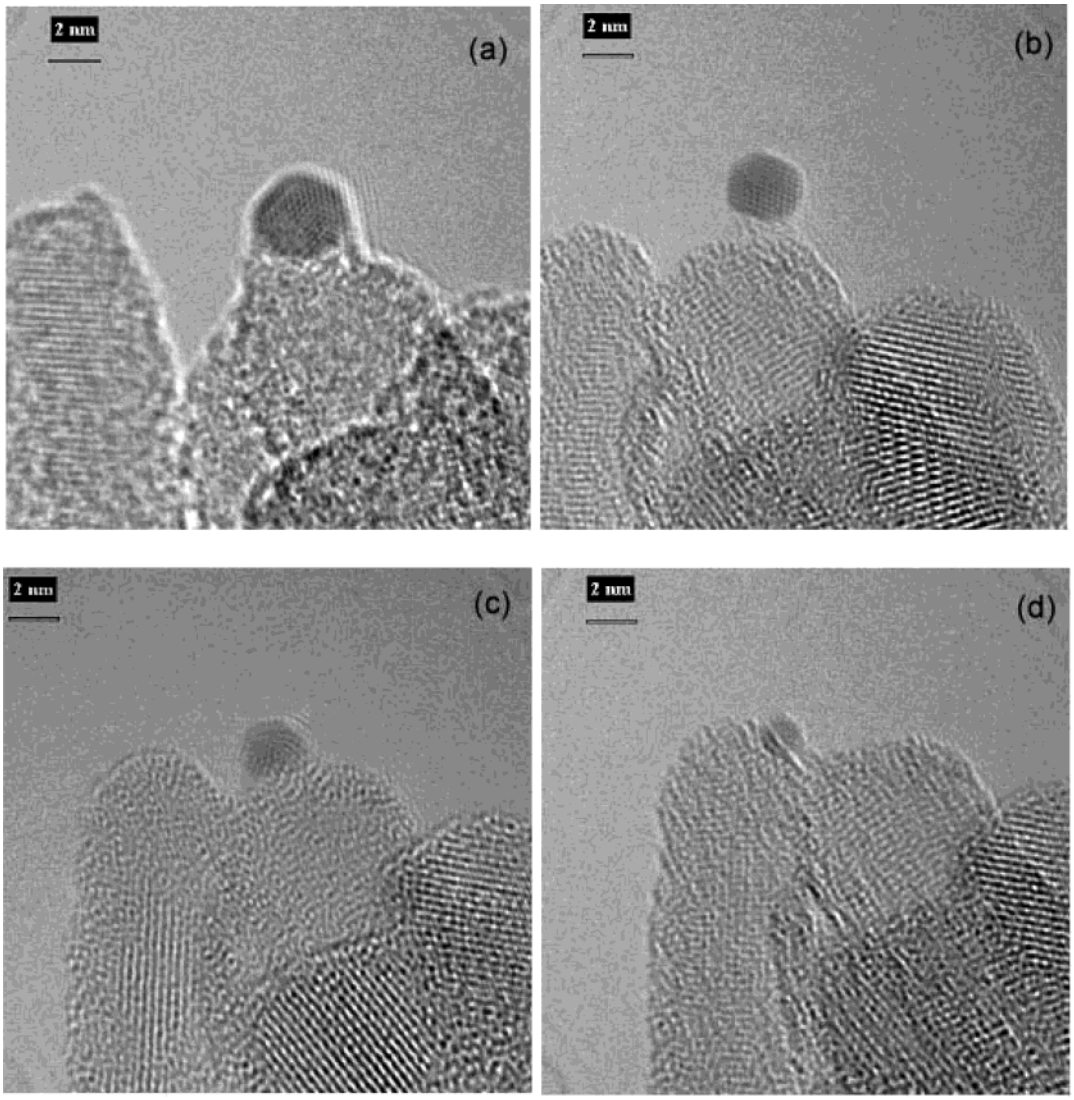

Figure 6. HRTEM image of the "sinking nanoparticle" process (a) in the beginning of the HRTEM observation; (b) and (c) in the process of the HRTEM observation; (d) after 1 min of HRTEM observation, the particle sinks beneath the surface of the oxide layer.

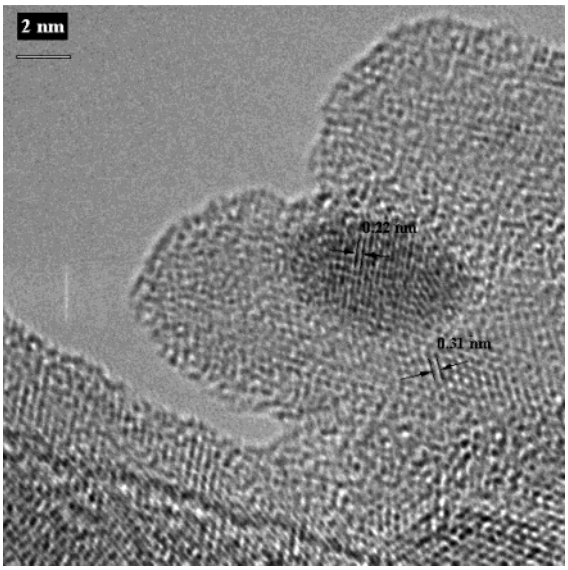

Figure 7. HRTEM image of an elliptical Pd nanoparticle with a short axis of 4 nm and a long axis of 6 nm on a SiNW surface.

samples is shown in Figure 11b. The Pd $L_{3,2}$-edges of Pd metal always exhibit an intense peak at the onset of the edge jump called the whiteline. It arises from a 2p to the unoccupied 4d band transition at the Fermi level (a dominant dipole channel). The postedge oscillatory pattern of the absorption coefficient results from the multiple scattering processes and is characteristic of the fcc Pd structure.[7,40,41] The XANES (X-ray absorption near edge structure) in the spectrum of Pd deposited from the 10^{-3} M solution exhibits a similar oscillatory pattern (arrows indicated in the spectra), while the spectrum of the 1.0×10^{-4}M sample suffers from poor statistics in the higher photon energy region as a result of dilution, lack of long range order in the presumably smaller nanoparticles, and chemical inhomogeneity. These spectra indicate that at least the 10^{-3} M nanodeposit is fcc crystalline Pd, consistent with the TEM observations. A close examination reveals that the Pd deposits from the 1.0×10^{-4} M solution exhibit a 0.9-eV threshold shift to the higher photon energy and a broadening in the width of the whiteline compared to Pd metal while the whiteline of the 1.0×10^{-3}M sample remains nearly the same. Both deposits have a slightly

(40) Sham, T. K. *Phys. Rev. B* **1985**, *31*, 1888.
(41) Sham, T. K. *Phys. Rev. B* **1985**, *31*, 1903.

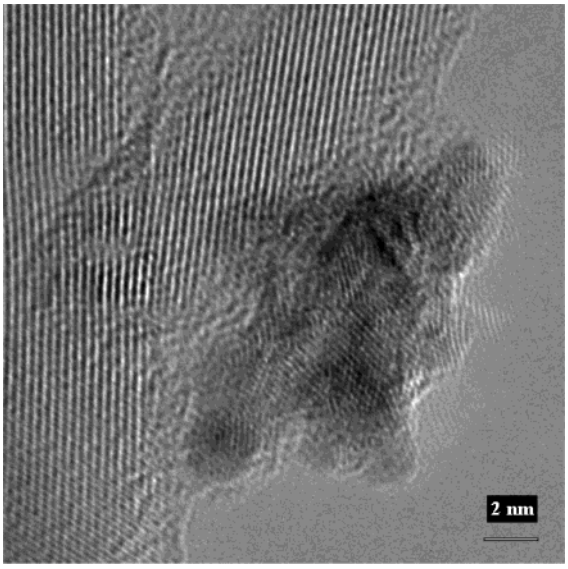

Figure 8. HRTEM image of an aggregate of several Rh nanoparticles of about 2 nm in diameter attached onto the surface oxide of SiNW.

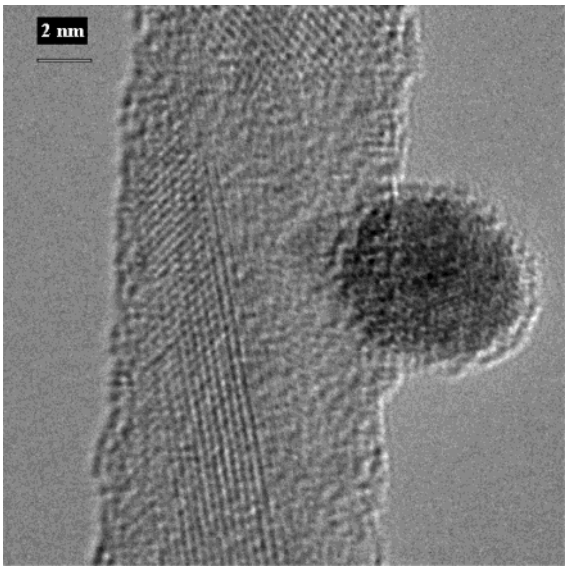

Figure 9. HRTEM image of a Rh nanoparticle "hanging" on the body of a SiNW.

broadened whiteline. The oscillations in the XANES of the 1.0×10^{-4} M sample appear to be noticeably packed, indicating a very disordered lattice and an increasing surface/interface contribution (Pd−O, Pd−Si contributions) which lead to increasing chemical inhomogeneity. On the basis of the TEM observation, we can definitely identify that the size of a majority of particles from the 1.0×10^{-4} M solution is smaller than 5 nm, while that from the 1.0×10^{-3}M solution range from tens of nanometers to hundreds of nanometers, less sensitive to nanosize effects. Thus, the blue-shift found in the 1.0×10^{-4}M sample is likely due to a combination of quantum size and surface effect of the smaller nanoparticles of Pd. The threshold shift is caused by d-electron count depletion in the Pd nanoparticles, which should be accomplished by an increase in the white line intensity.[40−42] This information cannot be extracted quantitatively from the 1.0×10^{-4} M Pd data, which suffer from poor statistics. However, the Rh results

(42) Mason, M. G. *Phys. Rev. B* **1983**, *27*, 748.

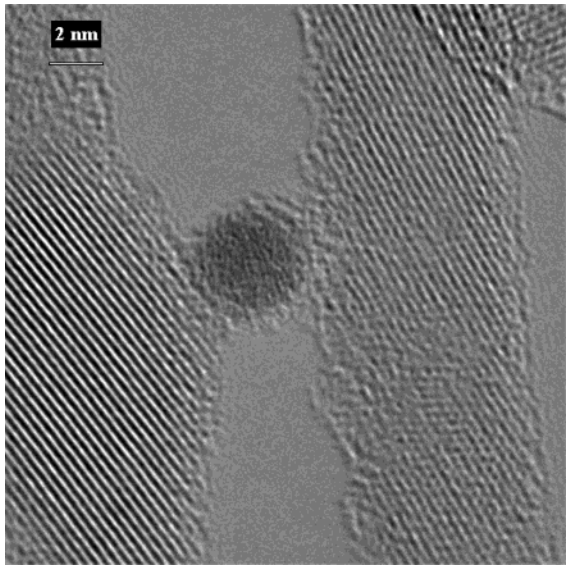

Figure 10. HRTEM image of a round Rh nanoparticle of 3 nm in diameter "sandwiched" between two SiNWs.

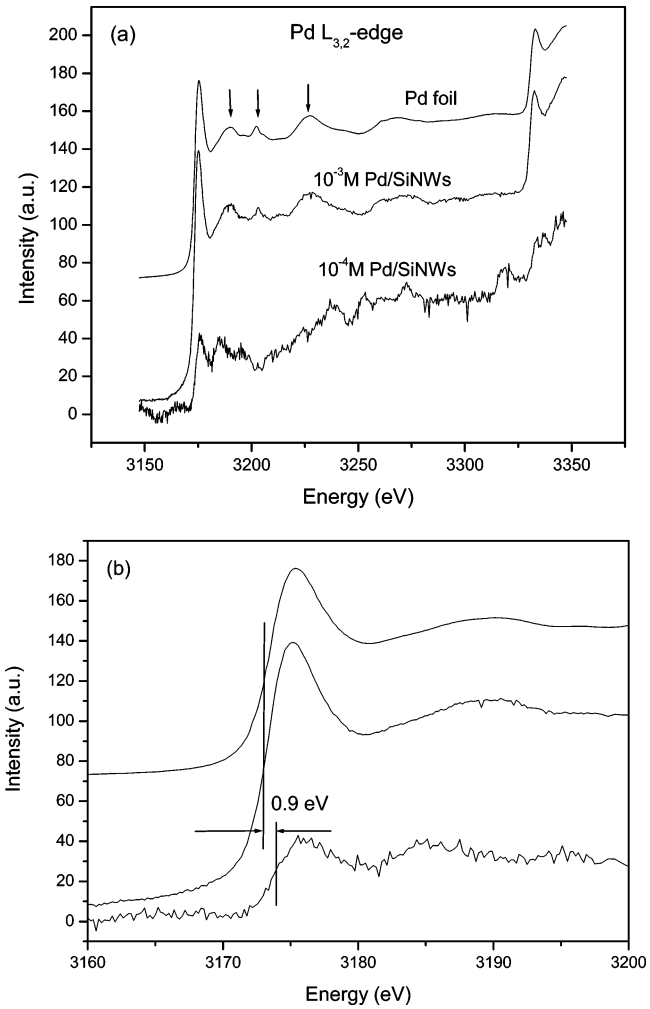

Figure 11. (a) Pd $L_{3,2}$ near-edge spectra of Pd/SiNWs compared with that of Pd metal. The spectra of the 1.0×10^{-3} and 1.0×10^{-4} M samples have been multiplied by a factor of 10 and 20, respectively. (b) A detailed comparison of the Pd L_3 near-edge threshold among the Pd structures as shown in (a).

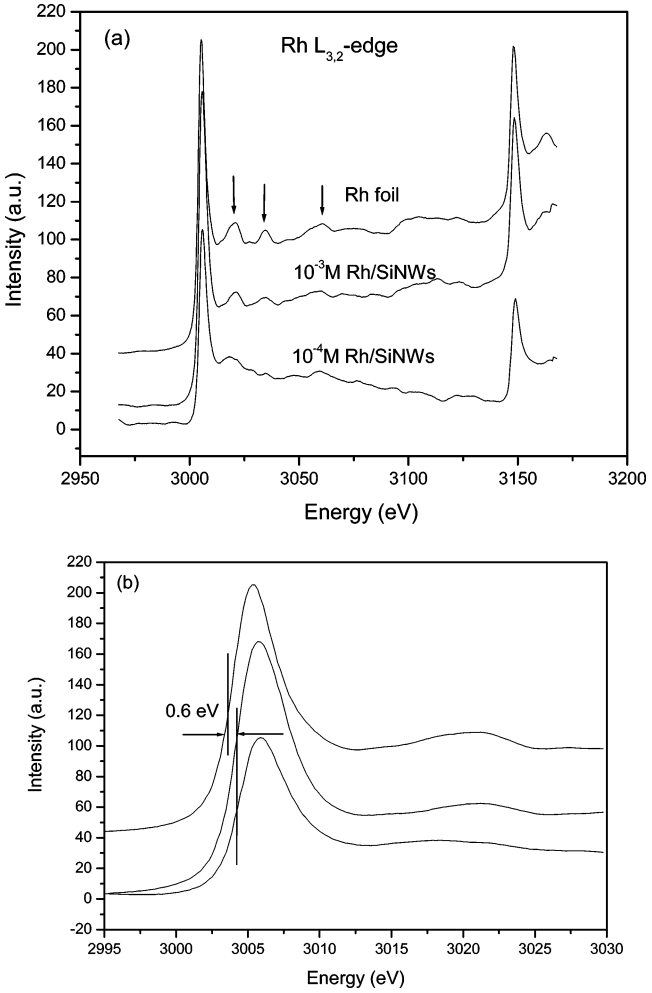

Figure 12. (a) Rh $L_{3,2}$ near-edge spectra of Rh/SiNWs compared with that of Rh metal. (b) A detailed comparison of the Rh L_3 near-edge threshold among the Pd structures as shown in (a).

(Figure 12) show a more noticeable trend. The white line widths are again slightly broader for the nanoparticles; the area under the curve for the Rh nanoparticles from the 10×10^{-3} M and the 10×10^{-4} M solutions are unmistakably several percentage points larger than that of the Rh metal foil and the threshold shifts to higher energy as the Pd nanoparticle size decreases (the lower the concentration, the smaller the nanoparticle). Thus, these data strongly support the presence of crystalline fcc nanoparticles as revealed by TEM; detailed quantitative spectroscopic analysis awaits better and a more complete set of data.

Figure 13 shows the Rh K-edge XAFS of two Rh nanostructures deposited on SiNW from a different batch of specimens prepared from a 10^{-2} M and a 10^{-3} M Na_3RhCl_6 solution with the same procedure. The XAFS of the Rh foil is also shown. The Fourier transform (FT) of the k^2 weighted EXAFS (extended X-ray absorption fine structures) is shown in the inset. We can see from Figure 13 that, despite a reduction in the amplitude of the EXAFS, the oscillatory patterns are identical. This provides unmistakable evidence for the presence of crystalline fcc Rh nanostructure, again

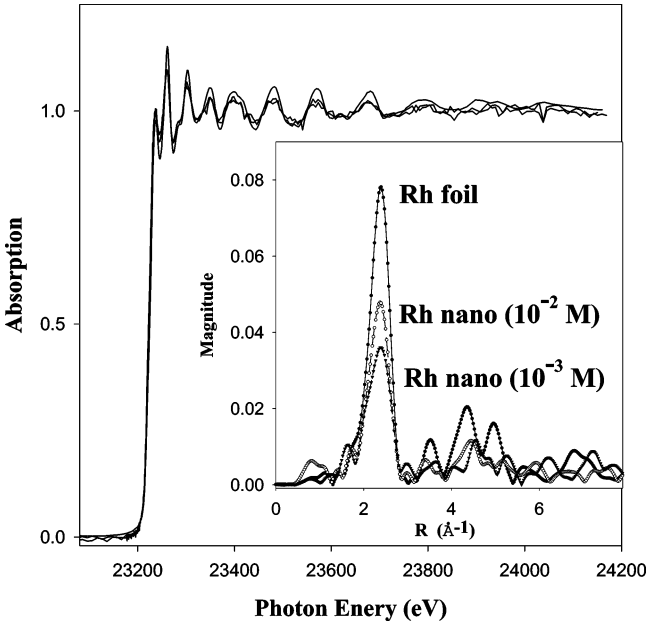

Figure 13. Rh K-edge XAFS of two Rh nanostructures deposited on SiNW from a different batch of specimens prepared from a 10^{-2} M and a 10^{-3} M Na_3RhCl_6 solution.

confirming the TEM observation. The FT clearly shows a nearly identical first shell with a noticeable size-dependent reduction in the amplitude and a slight asymmetry toward the smaller R region. This reduction is attributed to the degradation in long-range order, which is also reflected in the higher shells and increasing surface contribution (reduction in the coordination number and Deybe−Waller factor). The filtered back-transform of the first shell shows a slightly longer oscillation frequency for the nanostructures compared to the foil, indicating a possible contraction of the nanoparticle on average. More details of the analysis will be reported elsewhere. The Rh K-edge results clearly support that the nanoparticles are crystalline with an fcc structure.

The Si K-edge of the SiNWs at each stage of the reduction process was investigated. Figure 14 shows the Si K-edge XANES of a SiNW specimen following every stage of the treatment: from as-prepared to HF treatment and finally after the nanoparticle deposition with a 1.0×10^{-4} M Pd(II) solution. The near-edge region is shown in the inset. As noted above, the as-prepared SiNWs are encapsulated by a relatively thick oxide layer and are generally chemically inert. A controlled HF treatment was used to remove the Si oxide layer. The surface thus obtained was passivated with the formation of surface silicon hydrides that not only greatly inhibit surface oxidation in air[30,31] but also become a moderate reducing agent in the solution. It can be seen from Figure 14 that the as-prepared sample exhibits an intense resonance at ~1848 eV. This peak is characteristic of a Si 1s to 3p (t_2 orbital in a T_d symmetry) transition of SiO_2 and arises from the encapsulating silicon oxide layer of the SiNWs. The first resonance at ~1840 eV is associated with the unoxidized crystalline Si core of the nanowire. It is interesting to note that the as-prepared SiNWs exhibit a very strong SiO_2 peak, relative to the Si K-edge jump (white line) of the crystalline Si. This is due to a large ratio of surface Si (oxide) atoms to bulk (wire) Si atoms.[24] After HF

(43) McMaster, W. H.; Kerr Del Grande, N.; Mallett, J. H.; Hubbell, J. H. *Compilation of X-ray Cross Sections*; National Technical Information Services: Springfield, VA, 1969.

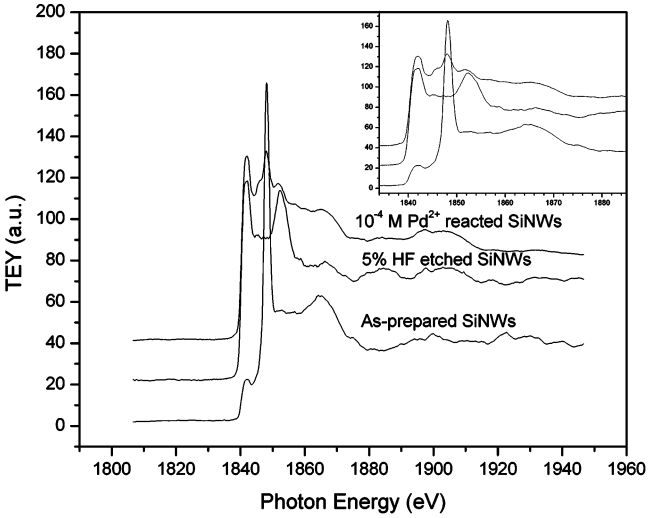

Figure 14. Si K-edge XANES of a SiNW specimen following different stages of treatment: as-prepared SiNWs, 5% HF etching, and after reaction with a 1.0×10^{-4} M Pd(II) solution. The near-edge region is shown in the inset.

treatment, the SiO_2 peak at ~1848 eV disappeared completely, and this was accompanied by an intense edge jump at ~1840 eV. This observation indicates that the Si oxide layer was removed completely by the HF treatment, that the SiNWs were elemental crystalline Si, and that the surface was passivated by hydrogen. Si−H EXAFS is difficult to detect on the huge background of crystalline silicon; however, the enhanced resonance at ~1853 eV is most likely associated with the presence of hydrides which enhance the forward scattering through the focused effect. Upon Pd deposition (10^{-4} M), the SiO_2 peak at ~1848 eV reappears together with a small low-energy shoulder at ~1845 eV. The shoulder at ~1845 eV can be clearly seen in the inset and is characteristic of silicon suboxide that presents most certainly at the silicon oxide and crystalline silicon interface. The silicon oxide results from surface reoxidization of the HF-etched SiNWs by the redox process involving the reduction of Pd(II) to metal in the solution. It confirms the above-reported TEM results that show Si oxides on the surfaces of SiNWs after deposition and further supports the proposed reaction process.

Finally, we report a preliminary experiment in which we attempt to prepare bimetallic nanoparticles by co-deposition of Pd and Rh from their mixed ions solution. Figure 15a and 15b show respectively the Rh $L_{3,2}$-edge and Pd $L_{3,2}$-edge results of nanoparticles deposited from Rh(III) and Pd(II) mixed solutions of different concentrations. Pd white lines in the two samples shifted to a high energy by 0.8 eV relative to the Pd foil but the Rh white lines remained unchanged. The oscillatory patterns above the white line in the Rh $L_{3,2}$-edge and Pd $L_{3,2}$-edge of the two samples exhibited a noticeable broadening, compared with the XANES of Rh and Pd foil, respectively. A comparison of the XANES in the sample deposited from a 50%−50% 5×10^{-4} M solution plotted in energy relative to the threshold is shown in Figure 16 together with a comparison of the L_3-edge jump for both metals. These features suggest that both Pd and Rh were reduced to metallic nanoparticles with an fcc structure (very similar oscillation patterns overall). Since both Pd and Rh have an fcc structure and

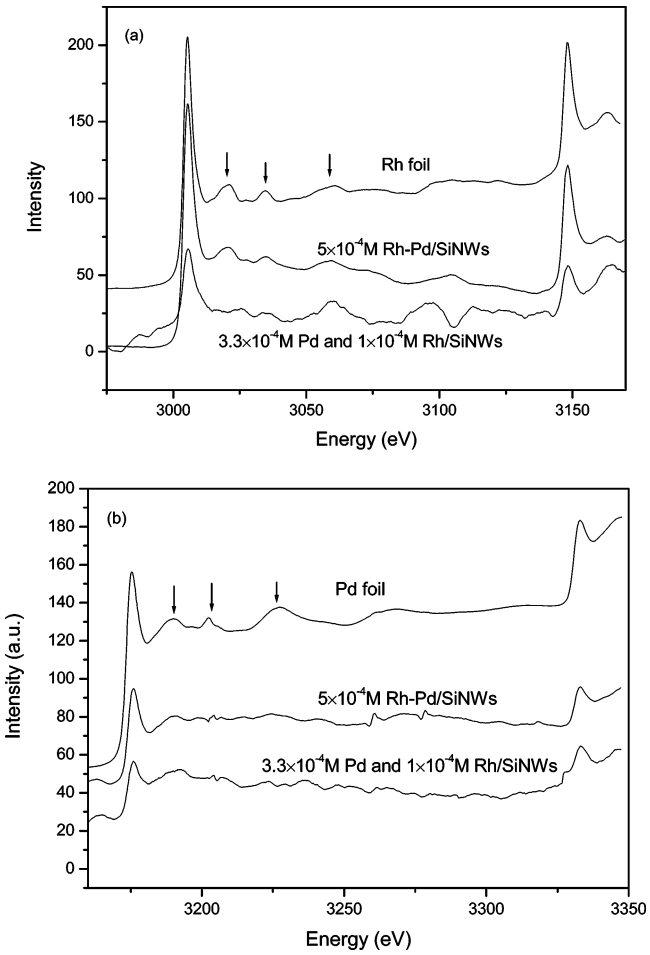

Figure 15. (a) Rh $L_{3,2}$-edge spectra of Rh−Pd bimetallic nanoparticles from Rh(III) and Pd(II) mixed solutions of different concentrations. (b) Pd $L_{3,2}$-edge spectra of Rh−Pd bimetallic nanoparticles from Rh(III) and Pd(II) mixed solutions of different concentrations.

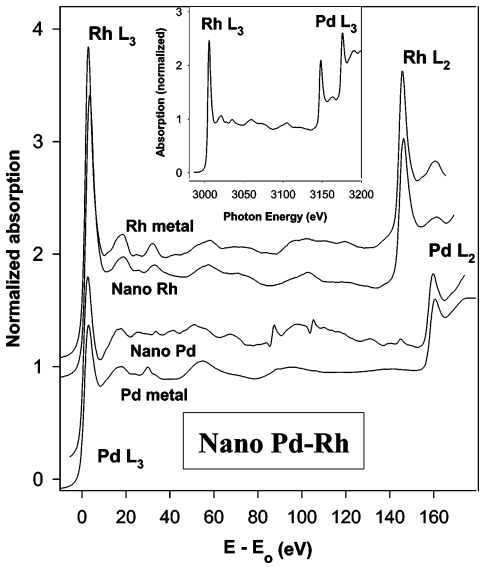

Figure 16. Comparison of the XANES in the sample deposited from a 50%−50% 5×10^{-4} M solution plotted in energy relative to the threshold.

their scattering phases and scattering amplitudes are very similar, we cannot conclude at present whether a bimetallic nanostructure is formed. The similarity in the oscillation pattern is not in favor of the formation of a

bimetallic random alloy, although it does not exclude the possibility of an fcc compound or the encapsulation of one metal by the other. Since the L_3-edge jump ratio of Pd to Rh in the nanostructure is 0.84 (inset), comparable to the atomic ratio of 0.92,[40] it suggests that Rh is slightly preferentially reduced by the SiNWs in this case. This is interesting considering that Rh requires three electrons to reduce to metal while Pd requires only two. Thus, this preliminary observation invites further investigation involving metal K-edge studies and the use of bimetallic Pd−Rh model compounds.

IV. Conclusions

Palladium and rhodium nanoparticles (<10 nm in diameter) have been fabricated on the hydrogen-passivated surfaces of SiNWs, which function as a moderate reducing agent for the reduction of Pd(II) and Rh(III) species in aqueous solutions to metal and a nanotemplate. The nanoparticles of various shapes such as round, elliptic, and polyhedral on the SiNW surfaces were observed under HRTEM. The larger nanoparticles (>5 nm) tended to adopt a round shape and were stabilized by a thin oxide layer; and the smaller nanoparticles (<5 nm) adopted polyhedral structures without an oxide layer. The smaller nanoparticles were unstable under the intense electron beam of the TEM. The two interesting phenomena of the "nanoparticle departure" and "nanoparticle submersion" processes as well as some interesting structures of the nanoparticles and the SiNWs were observed by HRTEM. It is envisioned that the fabrication of such metallic nanodots on nanowires will potentially lead to new and novel composite materials of importance in nanotechnology. The electronic properties and the local structures of the metal nanoparticles and SiNWs were investigated by XAFS. The Pd and Rh nanoparticles with a small diameter (<5 nm) clearly showed the size effect.

Acknowledgment. Research at the University of Western Ontario was supported by the Natural Science and Engineering Research Council (NSERC) of Canada. CSRF is supported by NSERC through a MFA grant and the National Research Council (NRC) of Canada. SRC is supported by the U.S. National Science Foundation under Grant DMR-00-84402. The PNC-CAT at APS, Argonne National Laboratory, is supported by the U.S. Department of Energy, Basic Energy Sciences, Office of Basic Science under Contract Nos. W-31-109-Eng-38(APS). N.-B. Wong acknowledges the support of a grant from the Research Grants Council of Hong Kong SAR (SiNWs RGC Grant 9040879 (cityu 1024/03)).

CM035112E